Unveiling the existence and role of a liquid phase in a high temperature (1400°C) pyrolytic carbon deposition process

Germercy Paredes, Thierry Ondarçuhu, Marc Monthioux, Fabrice Piazza

Carbon Trends 5 (2021) 100117

Contents lists available at ScienceDirect

Carbon Trends

journal homepage: www.elsevier.com/locate/cartre

Unveiling the existence and role of a liquid phase in a high temperature (1400 °C) pyrolytic carbon deposition process

Germercy Paredes[a,b], Thierry Ondarçuhu[c], Marc Monthioux[a,*], Fabrice Piazza[b]

[a] Centre d'Elaboration des Matériaux et d'Etudes Structurales (CEMES), CNRS, Université de Toulouse, Toulouse, France
[b] Laboratorio de Nanociencia, Pontificia Universidad Católica Madre y Maestra (PUCMM), Santiago de Los Caballeros, Dominican Republic
[c] Institut de Mécanique des Fluides de Toulouse (IMFT), CNRS, Université de Toulouse, Toulouse, France

ARTICLE INFO

Article history:
Received 31 July 2021
Revised 11 October 2021
Accepted 12 October 2021

Keywords:
Wetting
Nanoscale
Carbon nanotube
Graphene
CVD
Pyrolytic carbon

ABSTRACT

Based on experiments aiming at depositing pyrolytic carbon onto carbon nanotubes by means of a chemical vapor deposition (CVD) process at 1400 °C, the work we report here demonstrates that the deposition involves the transient formation of a liquid phase (here organic), and that wetting physics is still able to apply in spite of the high temperature and the nanoscale, *i.e.*, far beyond the condition range usually investigated. This was unexpected, because the high temperature makes all the physical and chemical processes involved transitory, including the fact that the liquid turns itself into solid carbon because of the ongoing carbonization process. The observations provide an estimate of the time scales of the involved processes, as they have to be short enough to complete in spite of the high temperature conditions. From a practical point of view, as the resulting material is a solid, all-graphenic carbon, the work demonstrates that using wetting physics in high temperature CVD can be a way to dramatically modify the surface energetics and the nano/microscale morphology of carbon nanofilaments. The statement is assumed to also apply to other chemical systems.

1. Introduction

Wetting physics is driving the way liquids behave when they meet solid surfaces, both in natural and technological processes. Wetting-related phenomena are usually investigated or used *(i)* at room or moderate temperature, *i.e.*, rarely higher that the range of curing temperatures for polymers; *(ii)* for macroscale down to microscale systems, *i.e.*, nanoscale is barely considered due to the experimental issues related to investigating nanosized liquid volumes; *(iii)* while involving a liquid whose chemical composition is different from that of the solid substrate, and which remains so, *i.e.*, the resulting material is somewhat heterogeneous. In the work presented here, investigating the processes involved in the deposition of carbon by means of thermal cracking of an organic precursor has unexpectedly turned out to be a way to investigate wetting phenomena beyond the experimental condition limits listed above.

The deposition of carbon by means of thermal cracking of a hydrocarbon gas or vaporized liquid feedstock has been used for decades [1–6]. When it is used to coat various materials with thin carbon films, the process relates to chemical vapor deposition (CVD). When it is used to infiltrate a porous preform, the process relates to chemical vapor infiltration (CVI) [4]. In both cases, when using conditions for which the gas phase is subjected to extensive homogeneous recombination reactions, the obtained carbon, so-called "pyrolytic carbon" or "pyrocarbon" (PyC), is graphenic with turbostratic structure, whatever the synthesis conditions used [2,4,6]. For favorable cases, the hexagonal (*i.e.*, Bernal) graphitic structure may be partially or fully obtained upon post-treatments (typically high-temperature annealing). The formation of PyC results from both homogeneous and heterogeneous processes in various proportions depending on the conditions [4]. Homogeneous processes refer to the reactions occurring within the gas phase, such as - in addition to the thermal cracking of the precursor gas - the recombination of radicals, atoms or molecular fragments, producing heavier species. On the other hand, heterogeneous processes are more thermodynamically favored [5]. They involve condensation reactions, where chemical reactions such as dehydrogenation and polyaromatization can take place at the contact of the substrate surface, and the adsorption/desorption of species onto and from the solid surface.

Depending on whether the homogeneous or the heterogenous reactions prevail, PyC exhibits different morphological and textural

* Corresponding author.
E-mail address: marc.monthioux@cemes.fr (M. Monthioux).

https://doi.org/10.1016/j.cartre.2021.100117

characteristics. PyC mostly resulting from homogeneous reactions shows overall isotropic textures whereas the prevalence of heterogeneous events tends to form more or less anisotropic (laminar) textures [4,6].

However, the vast majority of the studies on which the latter statements are based have involved substrates whose dimensions are very large with respect to the scale at which the chemical reactions and other events (such as adsorption) take place. Such a dimension ratio is indeed important, and it was already observed that the PyC local texture is deeply influenced by the local variations of the substrate topology, such as surface corrugations at nanoscale [7].

Unfortunately, very few extended investigations of the relationships between the structure, nanotexture, and morphology of PyC deposited onto CNTs and the deposition conditions have been carried out. For a long time, such a PyC deposition process onto MWCNTs was a common use to thicken MWCNTs into so-called vapor-grown carbon fibers (VGCFs) [8–10], but a full range of conditions which could have allowed revealing a large variety in the deposited morphologies was not explored. Recent works attempted to investigate the early steps of PyC deposition, but the synthesis conditions were not much varied either [11,12], and those steps are merely described in terms of depositing graphenes, which sounds too simplistic to account for the variety of conditions and PyC morphologies found in the literature. The deposition of PyC was also carried out to densify MWCNT preforms into C/C composites [13–15], but the observations regarding the deposition mechanisms were blurred by the fact that the CNTs were very close to each other, preventing any particular PyC morphology to develop.

However, few years ago, a thorough study dedicated to the deposition of PyC onto carbon nanotubes (CNT) was reported [16–19]. It showed the unprecedented formation of a variety of all-graphenic deposits with complex morphologies aligned along the individual CNTs, which were made up of either beads or fiber segments with rough surface, and fully developed or truncated cones with atomically smooth surface protruding from them. Recent examples produced in our lab are shown in **Fig. 1a–d**. The inner texture (*i.e.*, the way graphenes are displayed within the morphologies) is sketched on **Fig. 1e**, as determined in [18].

Understanding how such complex morphologies can form is not straightforward. Nevertheless, it was shown that the sequence of growth follows that reported in **Fig. 2** [19]. It was then clear that the first PyC deposits adopt a nanosized spindle-like morphology (Fig. 2a), and that the subsequent ones lead to the formation of fiber segments or beads (Fig. 2b,c).

What makes the PyC deposit to adopt the spindle morphology illustrated in Fig. 2a is a key question. The transient formation of a liquid phase at some moment in the furnace was proposed to be an important step of the deposition process [19], but this hypothesis was lacking strong support. With this paper, we bring further evidence for it and discuss about whether such a liquid phase exists, when and where it forms, and how it behaves.

2. Experimental

Experiments were conducted following conditions similar or close to those reported in [17]. Briefly, pieces of flexible graphite foil substrates are seeded by iron nanoparticles from a suspension in water, then dispatched on a refractory support along a horizontal piston-type ("plug-flow") CVD furnace. The furnace is first flown with Ar then pure H_2 while heating it up to 800 °C in order to reduce any iron oxide into metal iron, and then CH_4 is added while the temperature is risen up to 1100 °C in order to grow multiwall CNTs with outer diameters in the range of 5–10 nm. CNTs are coarsely aligned by the gas stream. This first step, obeying the catalyst-enhanced CVD (CCVD) mechanisms, is designated as the lengthening step. Then the temperature is risen again under pure Ar up to 1350–1400 °C, at which a mixture of CH_4 and H_2 is again introduced instead of Ar. This second step, designated as the thickening step, is obeying the CVD mechanisms, during which the complex morphologies mentioned in the introduction (**Fig. 1**) are formed during a 1–2 h dwell time. The CH_4/H_2vol ratio is in the range of 1/9 during the first step, and it is varied within the 1/2–1/4 range during the second step. The interest of the experimental set-up is that it includes a large isothermal zone several tens of centimeters long. Local conditions may thus vary only from the increasing residence time of the gas phase resulting in more extended homogeneous phase reactions while the gas phase proceeds towards the exhaust. This is why such specific CVD conditions were designated as "time-of-flight CVD" [17]. The time of flight of the species in the gas phase may be varied by adjusting the total incoming gas flow. As a matter of fact, the maturation of the gas phase increases with the time of flight, where "maturation" is a very convenient single word to designate the combined effects of temperature and time.

In principle, the thickening step could be applied to commercial CNTs instead of synthesizing our own CNTs as a first step, although this was never attempted. However, it is believed that synthesizing CNTs as a first step within the same furnace comes with three benefits: *(i)* it allows some control of the CNT alignment and straightness, as it is important for subsequent applications that the conical morphologies formed during the thickening step are aligned with respect to each other along the same CNT; *(ii)* it allows some control of the CNT density, as it is important that CNTs do not touch each other so that the PyC morphologies can fully develop; *(iii)* There is no contact with any atmosphere but that of the furnace between the lengthening and thickening steps, which could otherwise somewhat modify the chemical reactivity of the CNT surface with respect to the depositing species.

The PyC morphologies obtained were investigated by means of scanning electron microscopy.

3. Results and discussion

3.1. The common CVD deposition models

Three models for the formation of thin solid films from a vapor phase can be found in the literature [21,22]:

- the layer-by-layer mode, so-called the Frank-van der Merve (FM) growth model, in which the interaction between the substrate and the depositing species (adhesion) is much higher than the cohesion between the depositing species. A next layer will then grow only once the first layer is completed.
- the 3D-island-based mode, so-called the Volmer-Weber (VW) growth model, in which small clusters are nucleated directly on the substrate surface and then grow into islands as a condensed phase. The formation of islands takes place from the beginning of condensation, if the interaction energy between the depositing species (cohesion) is larger than that between the deposit and the substrate (adhesion)
- A mixture of both, so-called the Stranski-Krastanov (SK) growth model, in which a first layer-by-layer growth step is followed by the formation of 3D islands. The reason for switching the growth mode could be that the interaction of the second layer with the first layer is not as strong as it was between the first layer and the substrate. But many other reasons are possible [23].

Such deposition models are able to apply to a large variety of CVD-deposited materials. However, the three models mentioned above are often discussed in terms of atoms, *i.e.*, the depositing species are by far less large and complex than those involved in

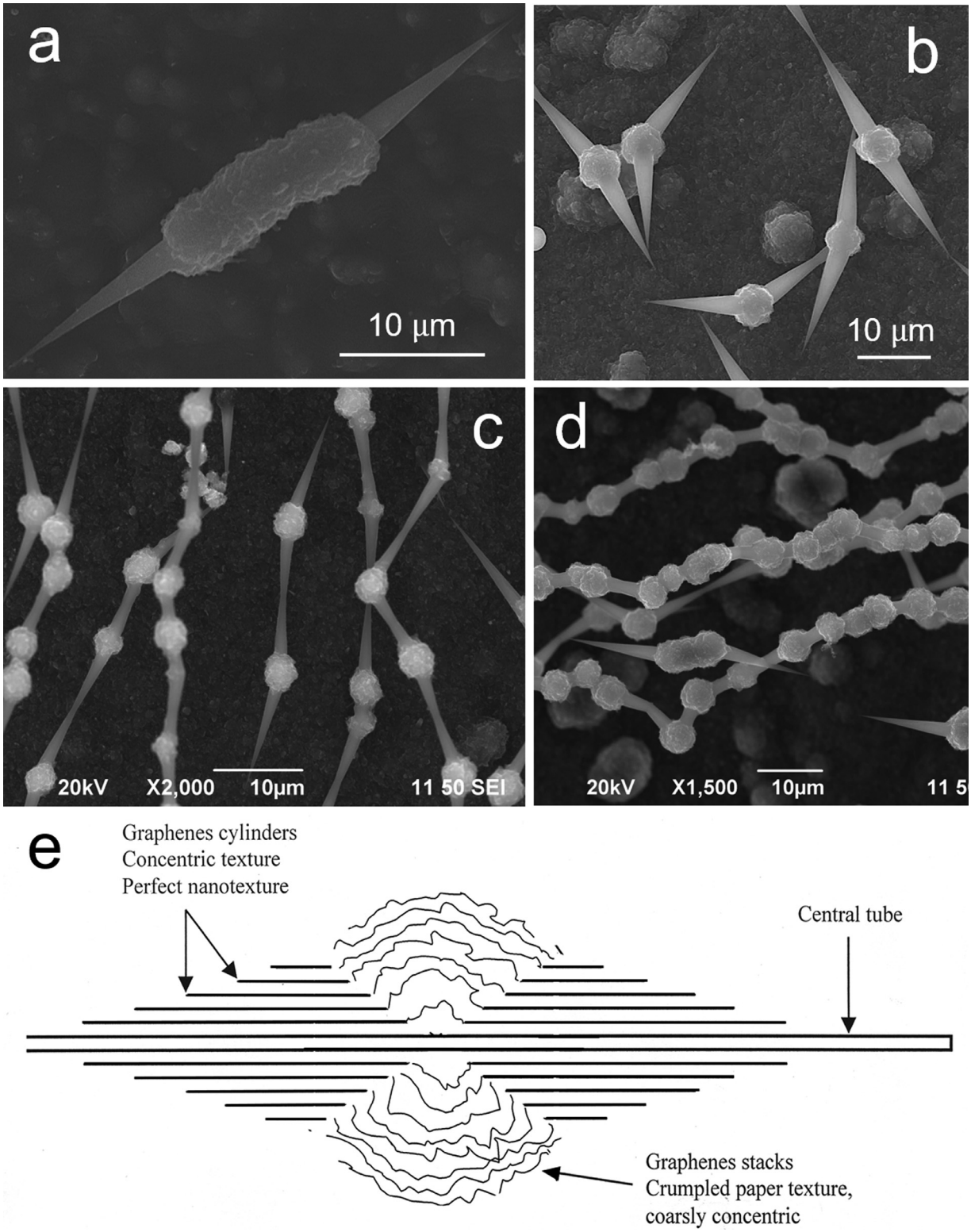

Fig. 1. Examples of the complex graphenic morphologies that form when PyC is deposited onto CNTs when the appropriate conditions are reached. **(a)** A rough-surface microfiber-segment with smooth-surface cones protruding at both ends. **(b)** Same as in (a), with a bead instead of a fiber segment. **(c,d)** Series of beads periodically displayed along their respective primary CNT and separated by truncated cone parts. Other examples can be found in [16–20]. **(e)** Sketch of the display of the graphenes constituting the morphologies as seen in cross-section. Image (e) is reproduced with permission [18] Copyright 2005, Elsevier.

our gas phase at high maturation level. In addition, two major differences make such models barely able to apply to our system: one is the substrate nature, *i.e.*, a nanosized filament, which has little to do with the kind of "flat" (*i.e.*, free of any step) surfaces usually considered when discussing the FM, VW; or SK deposition models; another is the fact that the chemical composition of the depositing species (hydrocarbons) evolves while the PyC is being formed, which may affect the adhesion *vs* cohesion force competition which seems to be the main driving factor. Despite these major discrepancies, based on the common observation that the de-

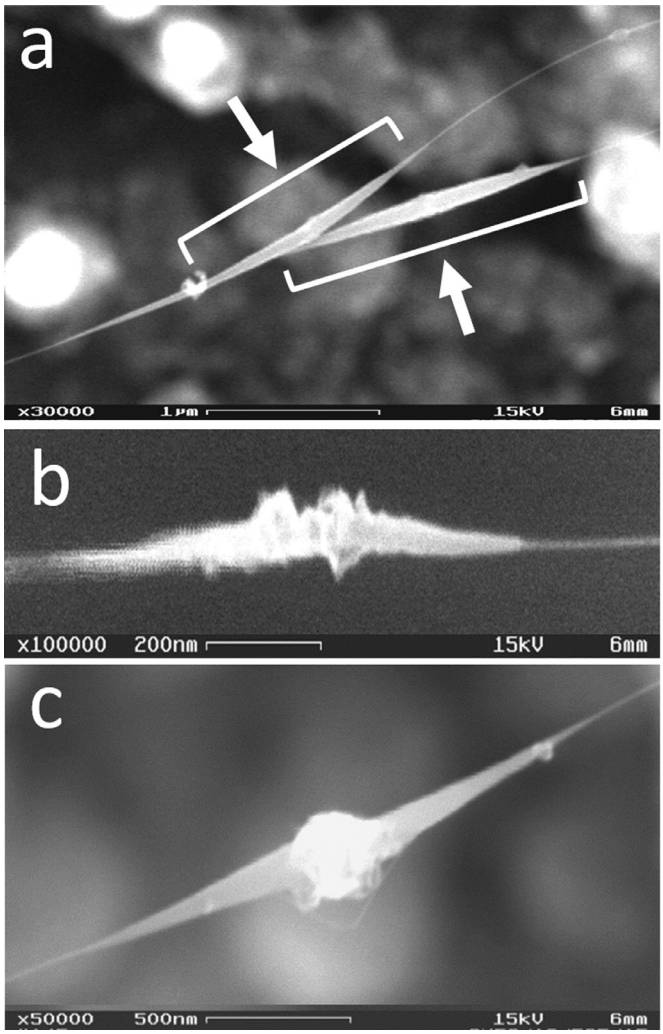

Fig. 2. SEM images showing the progressive occurrence of the cone-and-bead morphology of PyC when depositing onto a CNT. **(a)** Early deposition step results in the formation of spindle-like morphologies onto the nanotube surface (two of them are arrowed). **(b)** Then, the deposition becomes disordered once the thickest part of the double cone (*i.e.*, the cone base junction) reaches a threshold value of ~100 nm; **(c)** A bead starts to form. Reproduced with permission [19], Copyright 2006, Elsevier.

position of PyC starts with the formation of islands [24–26], Lee et al. [26] proposed that the deposition of PyC may follow the Volmer-Weber model. But the formation of the complex morphologies as illustrated in Figs. 1 and 2 which comprise both smooth- and rough-surface sub-morphologies with different inner textures and nanotextures growing at the same time constitutes a main objection to Lee et al.'s statement, as there is no way that the Volmer-Weber model may account for it. Furthermore, the local thickening conditions (which vary with the thickening time, time-of-flight, temperature, and CH_4/H_2 ratio) were shown to govern the thickness ultimately reached by the smooth surface cone-related sub-morphologies on the one hand, and by the rough surface sub-morphologies (beads or fiber segments) on the other hand, independently from each other. This is illustrated by **Fig. 3a** compared to **Fig. 3c** for instance, in which the development ratio of both sub-morphologies (*i.e.* the thickness and length variations of the beads or fiber segments over that of the fully/partially formed cones) is quite different.

This independence in the thickening behavior while both sub-morphologies grow in the same time demonstrates that they do not grow from the same species. Therefore, other scenarios have to be considered.

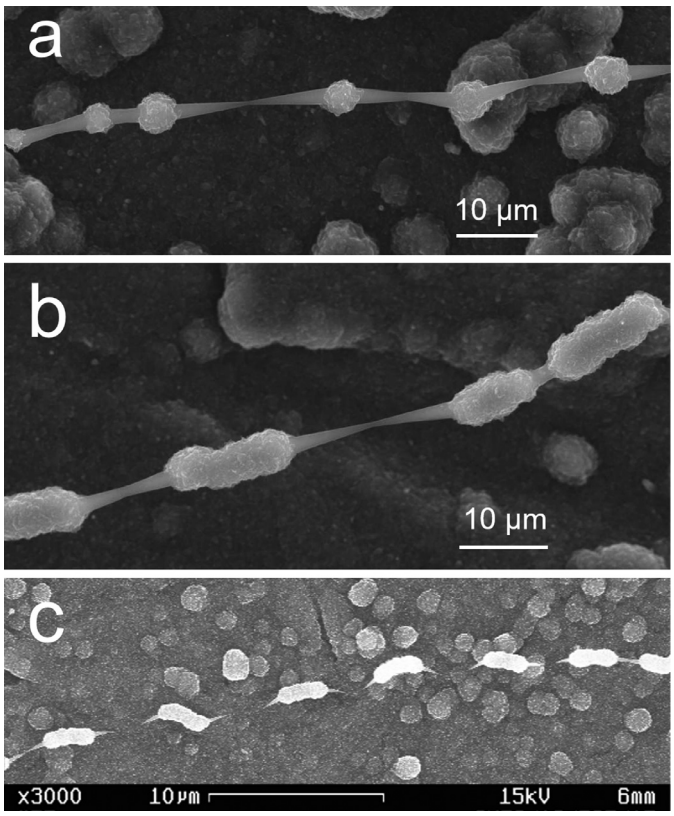

Fig. 3. **(a)** to **(c)** SEM images showing examples of the periodic display of the PyC deposits along their supporting CNT. Photo credit for image (c): H. Allouche (CEMES).

3.2. The existence of PAHs

As it breaks chemical bonds, thermal cracking generates radicals. However, the higher the residence time or time of flight, the more the radicals combine into new species, with some probability of the latter to also crack into radicals heavier than the primary ones. At some point, the gas phase has become a mixture of radicals and of molecular species resulting from their recombination. To account for the chemical complexity of the gas phase they had observed, a so-called "particle/filler model" was proposed by the Hüttinger's group [5,27–29]. This model assumed that polyaromatic hydrocarbons (PAHs) originating from polycondensation reactions of previously formed moieties are the "particles", whereas lighter, hydrocarbon molecules are the "filler", all of them resulting from the cracking and subsequent recombination events in various extent. The various PyC textures observed in the literature were proposed to result from various and specific particle/filler proportions. Importantly, PAHs are able to physisorb onto any surface, whereas radicals deposit through chemisorption, meaning that they require active sites to bond. This model was well-received and is now widely accepted, and even demonstrated by molecular dynamics [30]. The next question to answer is whether the PAHs deposit as such or as a liquid, wherever it forms.

3.3. The existence of a liquid phase

The particle-filler model originally did not consider the existence of a liquid phase, although the authors admitted it once as a possibility: "*Due to the slow rate of condensation reactions, the lifetime of the polycyclic aromatic hydrocarbons should be sufficient to permit the formation of a transient liquid and, in particular, a mesogenic film in which orientation processes are possible before carbon*

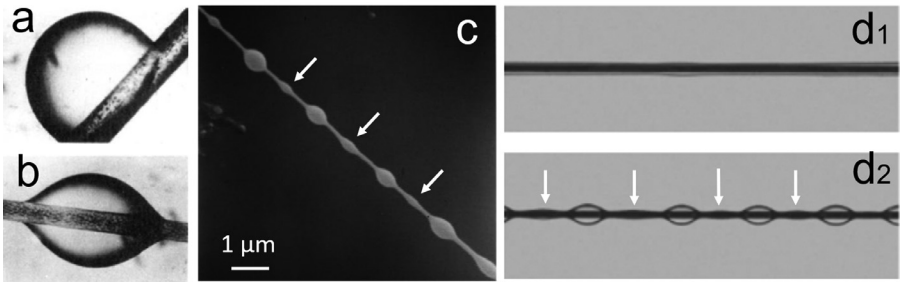

Fig. 4. **(a)** and **(b)** Effect of surface tension on the shape of a liquid droplet deposited onto a filament. (a) low-wetting conditions; (b) partial wetting conditions. In both cases the volume of liquid is the same, but the filament diameter is larger in (a) than in (b). Reproduced with permission [43], Copyright 1986, ACS Publications. **(c)** Droplet-like carbon morphologies lining-up periodically along a CNT, as obtained by Ting and Lan [45,46] after the formation of PyC onto CNTs from cracking CH_4 + H_2 at 1400 °C, as in our experiments. Reproduced with permission [46], Copyright 2000, Elsevier; the experimental conditions at which such a configuration was obtained cannot be ascertained, as the same image was said to correspond to 67.7% CH_4 and 10 min growth time in [46], and to 20% CH_4 and 30 min growth time in [45]; anyway, the similarity with (d2) is striking. **(d)** Example of the way a liquid film covering a fiber (d1) breaks up into a series of main and then subsidiary (arrowed) droplets (d2), upon the effect of the PRI (see text); reproduced with permission [47], Copyright 2008, IOP Publishing. The original images in (d) have no scale. Arrows were added to the original images of both (c) and (d2) in order to point out the occurrence of subsidiary droplet-like carbon morphologies (c) and subsidiary liquid droplets (d2) located between the main ones.

is formed" [27]. Meanwhile, they considered as "*relatively unimportant whether or not nucleation is based on the physisorption of individual species or on the physical condensation of aggregated species (droplets)*". Obviously, such a statement of unimportance regarding the actual existence of a liquid phase is scientifically irrelevant when investigating the early step of the deposition mechanisms of PyC onto nanosized filaments. Actually, Monthioux et al. [19] had to hypothesize that the PAHs species gathered into a PAH-rich liquid phase as the only way to account for several experimental observations: (*i*) the similarity between condensed-droplets and the PyC islands found in the early step of PyC deposition onto planar surfaces [24–26]; (*ii*) the meniscus-like morphology of the cones (yet solid) (see Fig. 9 in [19]); (*iii*) the axisymmetric geometry of the primarily formed spindle-like double cones as illustrated in Fig. 2a, which is a feature typical of droplets depositing on a string (an example will be provided later on, as Fig. 4b). The transient formation of a liquid phase was actually proposed long ago [31] and many times since then [2,3,23,32–35], but remained a matter of debate for long as the particle/filler model happened to prevail. Because the recombination reactions combined with secondary cracking in the gas phase certainly produce a variety of cyclic and non-cyclic hydrocarbons in their path to forming PAHs, the liquid phase was proposed to be similar to a pitch. Pitches are high molecular weight residues (possibly solid at room temperature) of either coal tar or petroleum distillation. As pitches are colloids in which PAHs are the micelles and light hydrocarbons are the suspensive medium [36], assuming the liquid phase in PyC deposition processes to be similar to a pitch made it compatible with the particle/filler model [19]. Therefore, the transient occurrence of such a liquid phase appears to be likely. This pitch-like liquid, once deposited onto the CNTs, carbonizes and transforms into PyC with the complex morphologies illustrated in Figs. 1 to 3. Of course, such a process has to be considered only for CVD conditions allowing it to take place, *i.e.*, allowing the gas phase to mature enough for generating PAHs and various other aliphatic hydrocarbons, typically by combining high temperatures with long residence times (or times of flight). Accordingly, other studies dealing with the deposition of PyC onto CNTs using non-suitable conditions did not result in the same complex morphologies [8–15].

3.4. The wettability of CNT surface by a pitch-like liquid

For the above-described scenario to happen, conditions for the total or partial wetting of the CNT surface by the pitch-like liquid phase should happen first. Dujardin et al. [37] determined that a liquid may wet CNTs until a cut-off value of its surface tension in the 100–200 mN/m range is reached. Pitches exhibit a large variety of chemical compositions coming along a large range (~40–300 °C) of melting or softening temperatures [38,39]. Correspondingly, they also exhibit a large range of surface tension values at molten state, from 27 to 320 mN/m, as well as a large range of viscosity, from 160 to 4000 cP [40,41]. Estimating the right surface tension and viscosity values of the depositing pitch-like liquid is difficult due to the out-of-equilibrium conditions involved, as evidenced by the fact that such a PAH-containing liquid exists at a temperature (~1400 °C) at which only a carbonized solid is supposed to be stable. Therefore, every scenario is possible: *(i)* either the lifetime of the species in the furnace is too short for allowing the formation of PAHs with heavy molecular weight, hence the liquid formed may exhibit viscosity and surface tension values corresponding to that of light molecular weight pitches (*e.g.*, in the range of below 1000 cP and below 50 mN/m, respectively [40]; as more familiar examples to compare with, the viscosity of water is 1 cP at 20 °C, that of fuels at 15 °C goes up to ~200 cP [42]); *(ii)* or the rapid carbonization of the organic liquid is promoted by the high temperature, making it rapidly behave like a high molecular weight pitch, hence with a fairly high viscosity (as a matter of fact, the temperature which marks the end of the regular primary carbonization process beyond which any organic precursor is irreversibly turned into a graphenic solid is as low as 450–600 °C); *(iii)* both previous scenarios may combine to generate a pitch-like liquid with any property value within the possible range. Overall, the range of pitch-like liquid characteristics is quite large, and covers the right range for allowing them to wet the CNT surface. When and where this liquid phase does form is the next question.

3.5. The two ways the pitch-like liquid phase could form

There are two ways for considering the occurrence of a liquid phase in CVD conditions: (*i*) the "mist analogy", which is a homogeneous phase process: the liquid phase forms within the gas phase as droplets prior to deposit onto the substrate (the CNT surface in our case), thereby making the gas phase a biphasic medium, made of both gas and liquid, similar to a mist. The droplet characteristics (number, size, aromaticity, viscosity) would be determined by the local conditions such as temperature, time of flight and composition of the gaseous feedstock; (*ii*) the "morning-dew analogy", which is a heterogeneous phase process: the liquid phase forms at the contact of the substrate surface following to a condensation mechanism similar to that which leads to the formation of the morning dew. Such a mechanism leaves the gas phase as a monophasic medium, which remains consistent with the par-

ticle/filler model. An important observation to make in order to sort-out between both hypotheses is that the complex PyC morphologies formed onto the CNTs, when not entirely covering them, tend to align somewhat periodically along them, regardless their development (Figs. 1c,d and 3). This, again, reminds the formation of water droplets onto the filaments of a spider web due to the condensation of the H_2O molecules contained in air, once the dew-point is reached.

The behavior of liquids depositing on strings should then be considered in order to find out which scenario applies.

3.6. Introducing the physics of wetting strings by liquids

3.6.1. The mist analogy

This scenario was hypothesized in [19]. In such a case, when a preformed liquid droplet deposits onto a filament, the surface tension drives the shape and configuration of the droplet which either adopts a non-symmetrical shape (**Fig. 4a**) or an axisymmetrical shape (**Fig. 4b**), depending on the droplet volume and the fiber radius respectively [43], that is to say the droplet over filament diameter ratio. The droplet shape can even be switched from axisymmetrical to non-symmetrical for a given filament diameter upon changing the liquid/filament surface interaction [44], which may happen if the liquid composition changes with time. Obviously, the primary spindle-like PyC morphology observed at the early times of the deposit (Fig. 2a) requires to originate from an axisymmetrical kind of droplet as in Fig. 4b, indicating that the CNT diameters are small with respect to the droplet diameters.

Whatever the scenario, it has to account for the periodicity of the display of the PyC morphologies deposited along the CNTs as shown in Figs. 1c,d, 3a,c, and other examples in [16,17,19]. It was hypothesized in [19] that it might relate to the statistical distribution of the droplets in the gas phase. The higher the concentration in droplets, the closer to each other the primary spindles (Fig. 2a) along a CNT, hence the subsequent cone-bearing morphologies which grow afterwards. However, a key result can be found in the images obtained by Ting and Lan [45]. In their attempts to reproduce the earlier work reported in [15] regarding the formation of cone-bearing PyC morphologies, these authors have obtained a deposition of PyC onto CNTs which definitely looks like a series of axisymmetrical droplets periodically dispatched along a string (**Fig. 4c**). Interestingly, smaller, subsidiary "droplets" (actually solid carbon) are seen between the large ones (arrows in Fig. 4c).

Such a configuration involving both main and satellite droplets cannot be explained by the deposition of preformed droplets. To explain it, another behavior of a liquid wetting a string called the Plateau-Rayleigh Instability has to be considered.

3.6.2. The morning dew analogy

Back in the XIXth Century, the Plateau-Rayleigh instability (PRI) was considered in order to explain the spontaneous deformation of a falling-down liquid cylinder until breaking into separated droplets once the fluctuation deformation wavelength (λ) is superior to the liquid cylinder perimeter ($2r$) [48]. The distance between the droplets being formed is determined by the fastest deformation mode (*i.e.*, the mode which takes the shortest time to develop). The PRI phenomenon is based on the liquid surface tension, main objective of which is to reduce the surface energy for the system to gain in stability while maintaining the same volume of liquid [48]. It may surely apply to PAH-rich liquids whatever their rheological properties, as according to [49], the same phenomenon can be also predicted to occur even with soft solids (polymers, colloids, gels) provided capillary forces are more important than elastic shear forces. The PRI plays the same way on liquid films supported by a filament (**Figs. 4d** and **5a**), hence it also relates to various natural phenomena such as the water droplets lining up on a spider web on morning dew as already mentioned above, as well as in some industrial applications such as fiber manufacturing, coating of optical fibers, surgical textile fibers, etc. [49]. However, for the PRI to play a role in such systems, gravity should be negligible, which is achieved as soon as the so-called Bond number $Bo << 1$ (the Gaucher number is also sometimes considered instead, such as $Bo = Go^2$), as expressed in **Eq. (1)**:

$$Bo = rgh_0{}^2/g \tag{1}$$

in which γ is the surface tension, ρ the density of the liquid, h_0 is the liquid jet radius (or represents (r + h), *i.e.*, the film thickness h added with the radius r of the supporting string when any), and g the gravitational acceleration. In practical, $Bo << 1$ occurs as soon as the filament radius is lower than ~50 µm according to Carroll [50], or even lower than a fraction of a millimeter according to Quéré [51]. In such a system, the species from the gas phase first condense onto the filament surface as a cylinder of a continuous liquid film (Figs. 4d1 and 5a1), and then the PRI enforces the film to break into axisymmetrical droplets (otherwise designated as "unduloidal" [48]) at a speed which depends on the liquid rheology and the fiber surface energy (Figs. 4d2 and 5a2-a3). Once the PRI has broken the primary liquid cylinder into unduloidal droplets, the latter are linked to each other by a thinner cylinder segment of liquid. Those subsidiary liquid films may also be subjected to the PRI effect, and generate new, smaller droplets located between the primary large ones [52], as illustrated by Fig. 4d2. Therefore, the PRI can explain the axisymmetrical shape commonly observed for the deposited droplets, their periodicity, and their regularity in various systems, from microscale [53] down to submicroscale [54] and nanoscale [55] (referring to the fiber radius). The similarity between systems as much different as polystyrene on glass fibers (**Fig. 5a3**), SnO_2 on Zn_2GeO_4 nanowires (**Fig. 5b**), and PyC on carbon nanofilament (Fig. 4c) is striking.

The key-parameters usually considered are the original thickness of the liquid film h, the wavelength λ of the unduloidal droplet display once the PRI effect has played (*i.e.*, the periodic distance between the aligned droplets), and the diameter $2r$ of the fiber. In the lubrication approximation ($R + h << \lambda$), these parameters are related as in **Eq. (2)** provided the liquid is non-viscous (inviscid conditions) [48]:

$$\lambda = 2\pi\,(r+h)\sqrt{2} \tag{2}$$

More generally, $\lambda = k\ (r + h)$ where k value ranges between 9 and 11 depending on whether h is small or high compared to r [52,56]. And then, considering our liquid film + CNT system, we may write **Eq. (3)**, thanks to Eq. (2):

$$h = \frac{\lambda}{2\pi\sqrt{2}} - r \tag{3}$$

Considering images such as Figs. 3a, c, and 4c, the periodicity observed between the cone-bearing morphologies along the CNT which supports them ranges from few µm up to ~20 µm, which then can be taken equal to the unduloidal wavelength λ. Considering a CNT radius r of ~5 nm, which is about a maximum according to our observations [17,20], Eq. (3) tells that the film original thickness h of the pitch-like liquid film covering the CNT should have been about 600 nm. Although no theory is going against such a hypothesis, that the furnace temperature of 1400 °C would allow the organic phase to deposit onto a CNT as a liquid film with such a large thickness (~60 times de CNT diameter!) all at once before it carbonizes sounds unlikely. Moreover, the subsequent PRI-driven breaking of such a liquid film would have generated unduloidal droplets of 2–3 µm in diameter, which is out of the dimension range found for the spindle-like morphologies which form

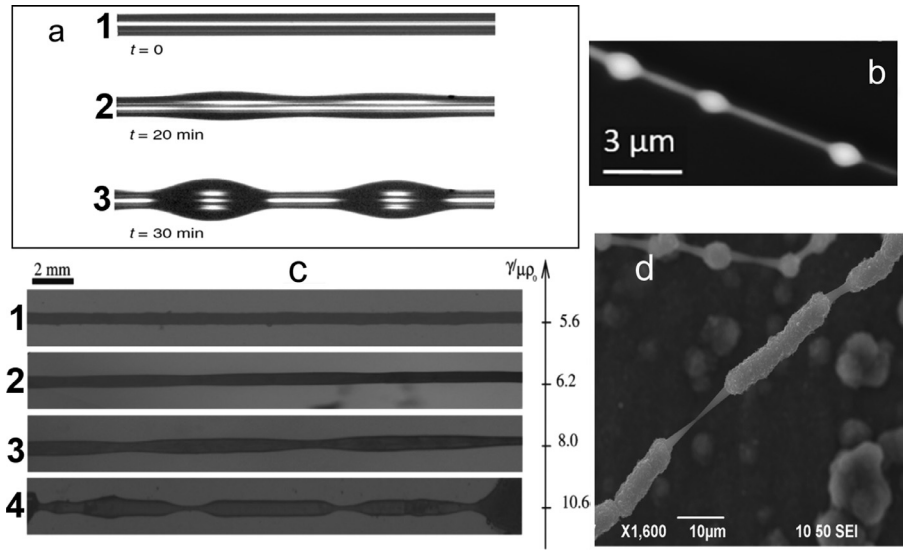

Fig. 5. Effect of surface tension on the shape of a liquid phase deposited onto a filament and then subjected to the effect of the PRI. **(a)** Example of a liquid polystyrene film wetting a glass fiber (fiber radius ~10 µm); at t = 0, initial film thickness was ~13 µm, and at t = 30 min, equilibrium is reached after the film has broken into axisymmetrical droplets periodically spaced; reprinted from [53] (CC BY 4.0 license). **(b)** SnO_2 beads lining-up onto a Zn_2GeO_4 nanowire obtained by thermal evaporation; reproduced with permission [54], Copyright 2020, ACS Publications. **(c)** Equilibrium shape of agar gel cylinders in toluene whose shear modulus was varied from 12 to 27 Pa from (c1) to (c4) by changing the proportion of water in the gel. Surface tension γ = 36.5 mN/m, µ = shear modulus, ρ_0 = initial cylinder radius; reproduced with permission [49], Copyright 2010, The American Physical Society. **(d)** Example of the PyC morphology obtained in conditions for which fiber segments preferably form instead of beads. Other examples are provided as Fig. 1a and 3b-c.

from the carbonization of the primary droplets, even considering the volume retraction which follows the liquid-to-solid transformation. Indeed, Fig. 2a shows spindle-like morphologies about 100 nm large at the thickest part. Considering a range of volume retraction of 40% for the most (*i.e.*, the upper limit for the volume retraction range for pitches upon carbonization (~5–40% for impregnation pitches [57]), the diameter of the droplets at the origin of the spindle-like PyC morphologies is not more than ~170 nm, *i.e.*, more than one order of magnitude lower than the value obtained when considering inviscid conditions.

This invalidates the assumption of inviscid condition used to derive Eqs. (2) and (3). This is not so much surprising as either the pitch-like liquid could be somewhat viscous by nature, depending on its chemical composition, or, for the least, is rapidly becoming so upon the effect of the high-temperature-induced carbonization (1400 °C in our case).

As the liquid viscosity was observed to be able to dramatically modify the unduloidal wavelength λ [58], viscosity should be introduced. Estimating the viscosity condition in wetting phenomena often refers to the so-called Ohnesorge number *Oh* such as:

$$Oh = \frac{\eta}{\sqrt{\rho\gamma h_0}} \tag{4}$$

where η is the dynamic viscosity, and the other parameters as defined above. Considering the range of values for pitches of η (160–4000 cP) and γ (27–320 mN/m) given above [40,41], and ρ < 1.5 [48], it is clear that $Oh >> 1$ in our system at nanoscale, which is the condition for which viscosity prevails over capillary forces in the way liquid jets or films break up. Furthermore, the unduloidal wavelength λ can be expressed in function of the *Oh* number as [47]:

$$\frac{\lambda}{h_0} = 2\pi\sqrt{2 + 3\sqrt{2}.Oh} \tag{5}$$

By combining **Eqs. (4) and (5)**, this allows writing, in first approximation, the following **Eq. (6)** [47]:

$$\frac{\lambda}{h_0} \simeq 2\pi\sqrt{2}\left(\frac{9}{2}\frac{\eta^2}{\rho\gamma h_0}\right)^{1/4} \tag{6}$$

Hence, λ/h_0 can be plotted in function of the viscosity η, as in Fig. 6:

Considering a viscosity value η in the range for pitches, *e.g.*, 1000 cP, Fig. 6 shows that a liquid film thickness of ~40 nm (subtracting the 5 nm CNT radius from h_0) is enough to obtain an unduloidal wavelength λ of 17.6 µm, *i.e.*, close to the ~20 µm illustrated in Fig. 3a. This is a much more plausible value than the ~600 nm calculated in the previous section when considering inviscid conditions. Another interesting result to consider is the range of the instability time τ_{instab}, that is to say the characteristic time needed by the PRI to operate at the selected wavelength. As reported in [47], for viscous liquids, τ_{instab} can be estimated through:

$$\tau_{instab} \sim 6\frac{\eta(r+h)}{\gamma} \tag{7}$$

As reported in the Table of Fig. 6, again taking the same example of a viscosity of 1000 cP, it can be seen that the PRI operates very rapidly, in the time range of 10 µs. This provides confidence that the pitch-like liquid deposited onto the CNTs gets enough time to break up into onduloidal droplets before being carbonized.

The spindle-like morphology of the primary PyC deposits (see Fig. 2a) appear very elongated with small conical angles. Assuming that this shape somehow reflects that of the primary axisymmetrical droplets resulting from the PRI, it could be that it is influenced by the way liquid films or jets break up at nanoscale. The breaking up mechanism is indeed dominated by the thermal fluctuations once the fluctuation amplitude is in the same range as the liquid film or jet dimensions [59,60]. The higher the thermal fluctuations (and they are assumed to be high in our system, considering the high furnace temperature – 1400 °C), the sharper the conical shape of the droplets ends, to the detriment of the thickness of the thin film left between the droplets.

Other wetting behaviors can also play to vary the shape of the primarily-deposited morphology to make it different from the spindle shape shown in Fig. 2a. For instance, the higher the surface energy of the filament supporting the same liquid, the more elongated and tapered the droplets [61]. Likewise, changing the rheo-

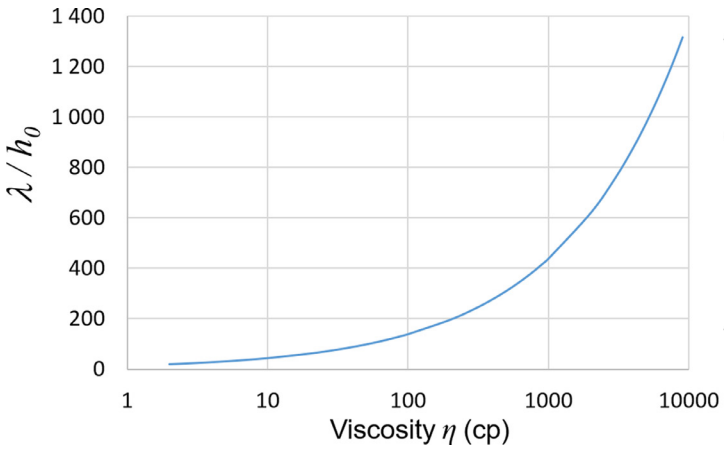

η [cP]	λ/h$_0$	h$_0$ [nm]	t [µs]
10	44	450	0,1
100	140	150	1
1000	440	45	10

Fig. 6. Plot of λ/h_0 ratio *versus* viscosity η using Eq. (6). In our system, h_0 may be replaced by $(r + h)$ (with r = CNT radius, h = thickness of the liquid film onto it. The Table shows some numbers extracted from the plot. The right-hand column provides the related instability time in viscid conditions, using **Eq. (7)**.

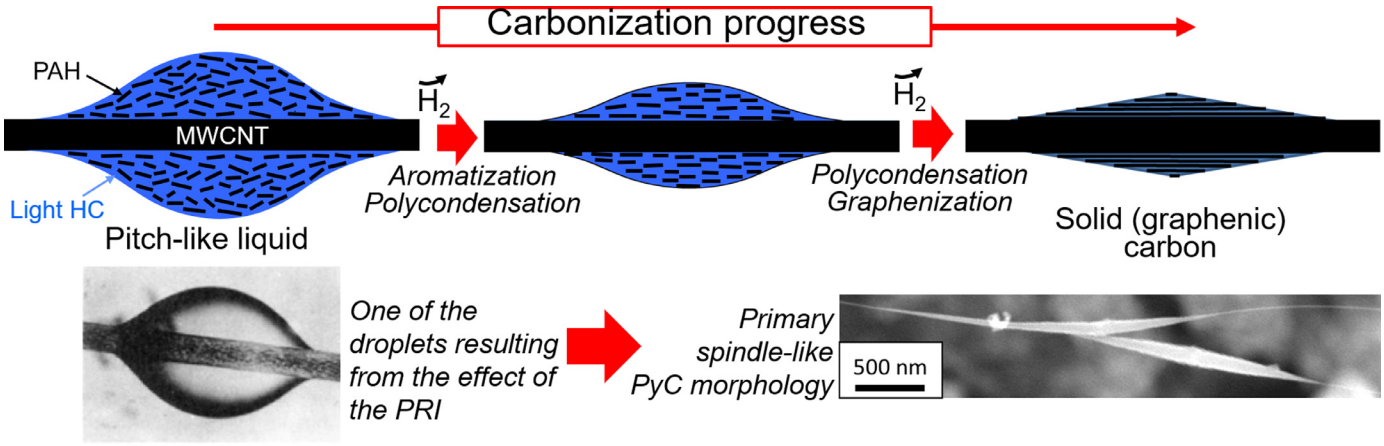

Fig. 7. Sketch (not at scale) of the morphological path from the rounded droplet originating from the PRI effect to the spindle-like PyC morphology resulting from carbonization.

logical properties of the liquid such as the shear modulus can also elongate significantly the shape of the unduloidal droplets up to making them "sausage-like" instead [49] **(Fig. 5c4).** Such primary sausage-like droplets could be at the origin of the elongated cone-bearing morphologies illustrated in Figs. 1a, 3b,c, and 5d Hence, the liquid viscosity plays a key role as it is able to modify both the morphology of the droplets and the unduloidal distance between them [58]. Overall, the main motor of the tapering of the primary PyC morphologies while starting from round-shape droplets could merely be carbonization (**Fig. 7**).

The axisymmetrical droplets resulting from the PRI as sketched on the left of Fig. 7 are in condition of partial wetting, meaning that surface tensions are high at the interfaces. Then, because of the progress of the carbonization which induces the vanishing of the light hydrocarbon components of the droplets, and induced the polycondensation of the PAHs, the droplets reduce in size, thereby enhancing the effect of interfacial stresses and enforcing more and more of the PAHs to align with respect to CNT surface, as already proposed in [19]. This is the same process that makes graphitizable a non-graphitizable polymer such as Kapton provided it is spread out as a thin layer [62]. Ultimately, the carbonization is completed and the aligned PAHs generate perfect, concentric graphene cylinders, as imaged in [18]. The carbonization is certainly completed rapidly, because of the 1400 °C of the furnace, *i.e.*, in the range of few seconds. An interesting comparison can be made with the images found in [63], which show MWCNTs periodically covered with droplet-like amorphous carbon beads as a result of electric arc MWCNT synthesis experiments. In such conditions, only carbon atoms are present (in addition to Ar, the plasma-forming gas). Therefore, the carbon beads could only result from the solidification of molten carbon droplets (as enabled by the very high temperature at the cathode, typically 6000–8000 K). As a consequence, a colloid-like system involving PAHs could not form, and the molten carbon droplet volume could not shrink either, because no carbonization process was going on, and only a state transition from liquid to amorphous solid took place instead. In addition, the images in [63] are much more alike those in [45,46] (see Fig. 4c) instead of ours, *i.e.*, the cone/bead discrimination could not occur in Ting's experiments despite the system is similar to ours (temperature, feedstock, MWCNT substrates). The reason is certainly that the organic liquid formed in Ting's experiments did not get the chance to become colloid-like, due to the difference in the experimental conditions and specifically the lack of long times-of-flight which are enabled in our system, and which are necessary to promote an extended maturation of the gas phase.

Finally, it is reminded that the final step of our PyC deposition process to obtain morphologies as illustrated in Figs. 1 and 3 corresponds to a dwell time of 2 h, during which the gas phase composition remains the same. Therefore, the pitch-like liquid phase forms continuously onto the CNT surface. It is surprising, then, to observe that the supporting CNT may not be fully covered by PyC after a while, as in Figs. 1b and 3c for instance. The explanation may relate to the behavior of a liquid when wetting a string whose diameter is not constant. The difference in diameters cre-

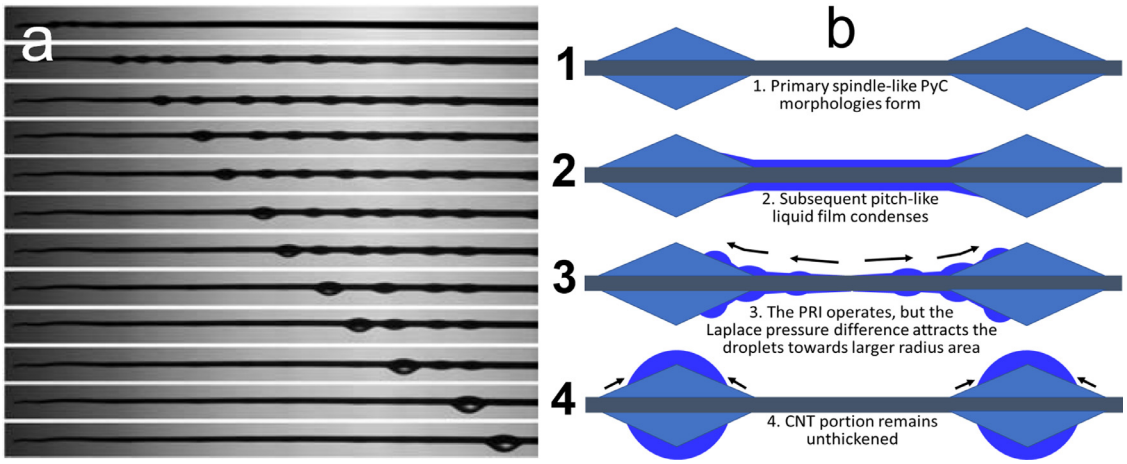

Fig. 8. **(a)** Behavior of a liquid film (here, silicon oil) deposited onto a conical string (with the radius increasing from left (100 µm) to right (300 µm)). From top to bottom (5 s between each image): first image, deposition of the liquid film; second image, the PRI operates; following images, the liquid is attracted towards the larger radius area; reproduced with permission [64], Copyright 2004, Cambridge University Press. **(b)** Sketch (not at scale) of the same effect as in (a) applied to a CNT after the formation of the first spindle-like PyC morphologies; Step b1 corresponds to the final step in Fig. 7; Step b2: a pitch-like liquid film condenses onto the CNT surface; Step b3: The PRI breaks the liquid film into droplets, but the difference in Laplace pressure between both ends of droplets lying across areas exhibiting a diameter difference (at the cone/CNT interface) makes them move towards the area of larger radius, thereby dragging in the same direction the other droplets still left on the CNT (area of equal diameter); Step b4: the liquid gathers at the thickest part of the spindle, foreshadowing the cone-bearing bead morphologies of PyC as sketched in Fig. 1e. Of course, the liquid also forms onto the spindle surface meanwhile, but is subjected to the same effect. It is not drawn for clarity.

ates a difference in the Laplace pressure which the liquid object is subjected to, which induces the liquid to move towards the string region of larger radius (**Fig. 8a**) [64,65]. This mechanism is currently exploited to enhance the trapping of condensed water and collecting it from mist [66]. It is a key statement for our system as it definitely eliminates the hypothesis of the deposition of preformed droplets (the mist analogy), which is not able to explain why droplets would not subsequently deposit on the CNT portions located between two previously formed spindles. As the conical parts grow in the mean time thanks to the contributions of the radicals as discussed in [19], this mechanism can keep going as long as the cones are not fully covered by the carbon coming from the carbonized liquid, which ends up by exhibiting a bead morphology as in Fig. 1b-d and 3a, or a fiber segment morphology as in Figs. 1a, 3b,c and 5d This is consistent with the earlier observations which showed that the "bead" or "fiber segment" part tends to overlap the cone part [18]. This mechanism also remains consistent with the assumptions proposed in [19] which explained the poorer graphene alignment in the "bead" of "fiber segment" part by the fact that the PAHs contained in droplets in low wetting conditions as imaged in Fig. 4a are subjected to limited interfacial stresses (as opposed to what happens in axisymmetric droplets as described in Fig. 7). This poor alignment of the graphenes is also responsible for the rough surface aspect (as opposed to the cone surface, whose roughness is at the atom scale [18] because the feeding species are only small radicals).

A comprehensive scenario may now be given as sketched in **Fig. 9** (considering a single CNT and incremental steps for clarity, although the continuous feeding of the gas phase over the whole dwell duration makes the phenomena continuous as well):

Step 0: starting situation: a CNT is present, along with a gas phase containing small radicals (possibly with a prevalence of carbon atoms), PAHs, and light hydrocarbons

Step 1: a pitch-like liquid condenses onto the CNT surface as a liquid cylinder of nanosized thickness

Step 2: in the range of microseconds, the PRI operates and breaks the liquid cylinder into nanosized rounded or "sausage-like" droplets, depending on the liquid rheology. The appropriate droplet/CNT diameter ratio and/or the CNT surface/liquid phase interfacial tension make that droplets are in conditions of partial wetting, making them axisymmetric. Because of the thermal fluctuations possibly combined with the right liquid rheology and the effect of the carbonization (see Fig. 7) the droplets are not rounded but exhibit tapered ends. Meanwhile, the PAHs contained in the droplets align parallel to the CNT surface because of the stresses induced by the surface tensions.

Step 3: the droplets carbonize into concentric graphenes whose length is as shorter as the diameter is larger, resulting in the primary spindle-like solid carbon morphology. The spindle surface is made of graphene edges (also see Fig. 1e), now able to play the role of active sites enabling the chemisorption of radicals.

Step 4: as the gas phase is continuously fed, liquid films keep condensing everywhere (*i.e.*, both onto the primary spindles, and on the naked CNT parts). The liquid which happens to condense on thickened parts (right column of the sketch) cannot form a film because the droplet/nanotube diameter ratio is modified. The PRI can no longer operate, and the wetting conditions switch from the case of Fig. 4b to that of Fig. 4a.

Step 5: those liquid films behave differently than the primary one (formed at *Step 1*) because they deposit onto a nanofilament with diameter variations, which makes that the droplets formed as resulting from the PRI are then attracted to areas of larger diameter, *i.e.*, the middle of the spindles (left column of the sketch) or to both ends of the carbonized sausage-like morphologies (right column of the sketch).

Step 6: all the liquids are now gathered onto the parts of larger diameters, leaving the previously-naked CNT parts naked again.

Step 7: the condensed liquid carbonizes while the PAHs contained are poorly aligned, generating the poorly aligned graphene texture and rough surface. Meanwhile, since Step 3, cone parts may grow from the radicals.

From this moment, Steps 3 to 7 repeat all along the duration of the dwell time.

Overall, the most important parameters for allowing the peculiar PyC morphologies illustrated in Figs. 1 and 3 to form are certainly the joint existence and proportions of the condensed liquid phase and of small radicals. Commenting this further would be too much speculative because of the lack of related experimental data,

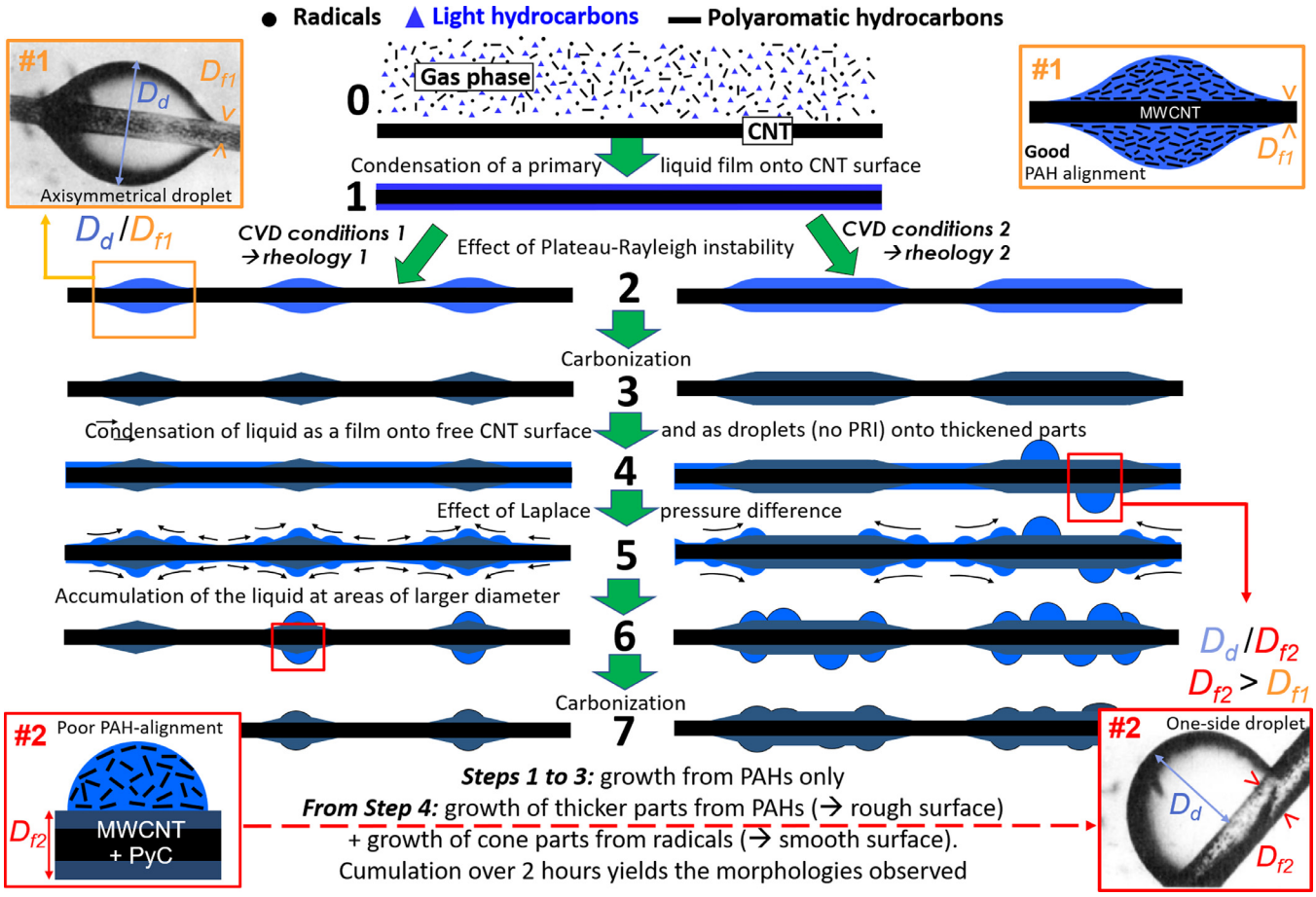

Fig. 9. Sketch (not at scale) summarizing the mechanisms of PyC deposition onto carbon nanotubes in a Time-of-Flight CVD process. D_d = Diameter of droplet; D_{f1}, D_{f2} = diameter of filamentous substrate, with $D_{f2} < D_{f1}$.

but several scenarios could be thought of in order to account for the large variety of CNT-supported PyC morphologies which can be obtained as described in [9], which would be worth investigating.

4. Conclusions

When pyrolytic carbon (PyC) is deposited onto carbon nanotubes (CNTs) as substrate, periodically-aligned, complex and peculiar PyC morphologies can form, following mechanisms which have remained poorly understood or poorly demonstrated for long. Comparing the various observations that could be made and the literature dealing with the dynamic behavior of liquid jets and films resulted in revealing that the primary mechanisms driving the formation of these PyC morphologies follow the same physics laws which drive the wetting of strings by liquids at submillimeter-scale down to microscale. This work then provides the demonstration that the physics of liquids wetting strings is still able to operate at very high temperature (1400 °C) and at nanoscale.

From the point of view of carbon material science, all the observations reported here concur to state that:

- the deposition process starts with the condensation of the organic species present in the gas phase as a pitch-like liquid phase, *i.e.*, containing polyaromatic hydrocarbons (PAHs) and smaller molecules;
- this liquid phase does not form droplets in the gas phase (the mist analogy), but condenses as a liquid film around each of the CNTs (the morning dew analogy);
- this liquid phase is subjected to the same physical phenomena as any other liquid wetting a string, *i.e.: (i)* it breaks up into periodically-aligned axisymmetrical droplets under the effect of the Plateau-Rayleigh instability, before the droplets carbonize into primary spindle-like PyC nanoobjects; *(ii)* in order to be consistent with the dimensional characteristics observed, the liquid has to be viscous (characterized by an Ohnesorge number $Oh >> 1$), which is consistent with its pitch nature, and its rapid transformation into a solid upon carbonization; *(iii)* the morphology of the axisymmetrical droplets can be modified according to the rheology of the liquid, in particular the viscosity, and in particular because of the nanoscale, so that to match the morphologies observed; *(iv)* when deposited onto a CNT with diameter variations, the pitch-like liquid is attracted to the areas of larger radius, explaining why the periodically-displayed PyC morphologies can keep growing while leaving uncovered the CNT parts in-between; *(v)* the same reason explains the preferred formation of the rough-surface bead morphology at the largest part of the primary spindle-like PyC objects.
- after primary axisymmetrical droplets have formed and then carbonized, the smooth-surface conical parts and the rough-surface bead or fiber-segment parts from which the conical parts protrude grow independently, hence supporting the hypothesis that they do not grow from the same species; typically, radicals prevail for growing the cone parts, whereas PAHs prevail for growing the rough parts.

Finally, in addition to demonstrating the transient existence of a liquid phase in PyC deposition processes (at least for CVD processes involving atmospheric pressure and long residence times or times-of-flight), the work opens the door to a wetting-controlled

engineering route for tailoring the morphology and surface energy of carbon nanofilaments. It is probable that this engineering route should also work for chemical systems other than carbon-based, for instance silicon-based, provided the same kind of reaction chain may occur and that sufficient time is given for allowing multiple recombination to take place until species condensable into liquid can form.

Declaration of Competing Interest

The authors declare that they have no known competing financial interests or personal relationships that could have appeared to influence the work reported in this paper.

Acknowledgements

This study has been supported through the EUR grant NanoX n ANR-17-EURE-0009 in the framework of the "Programme des Investissements d'Avenir". The Pontificia Universidad Católica Madre y Maestra (Santiago, Dominican Republic) is also thanked for providing the PhD grant for GP.

References

[1] R. Diefendorf, The deposition of pyrolytic graphite, J. Chim. Phys. 57 (1960) 815–821.
[2] J.C. Bokros, Deposition, Structure and Properties of Pyrolytic Carbon, in: P.A. Thrower, J.M. Walker (Eds.), Chemistry and Physics of Carbon, Deposition, Structure and Properties of Pyrolytic Carbon, 5, Marcel Dekker, 1969, pp. 1–118.
[3] P.A. Tesner, Kinetics of Pyrolytic Carbon Formation, in: P.A. Thrower (Ed.), Chemistry and Physics of Carbon, Kinetics of Pyrolytic Carbon Formation, 19, Marcel Dekker, 1984, pp. 65–161.
[4] P. Delhaès, Chemical vapor deposition and infiltration processes of carbon materials, Carbon 40 (2002) 641–657.
[5] K.J. Hüttinger, CVD in hot wall reactors - The interaction between homogeneous gas-phase and heterogeneous surface reactions, Chem. Vap. Dep. 4 (1998) 151–158.
[6] A. Oberlin, Pyrocarbons, Carbon 40 (2002) 7–24.
[7] J.F. Després, M. Monthioux, Mechanical properties of C/SiC composites as explained from their interfacial features, J. Eur. Ceram. Soc. 15 (1995) 209–224.
[8] M. Endo, Grow carbon fibers in the vapor phase, Chemtech 18 (1988) 568–638.
[9] A. Oberlin, M. Endo, T. Koyama, Filamentous growth of carbon through benzene decomposition, J. Cryst. Growth 32 (1976) 335–349.
[10] X. Lin, W. Zhao, W. Zhou, P. Liu, S. Luo, H. Wei, G. Yang, J. Yang, J. Cui, R. Yu, L. Zhang, J. Wang, Q. Li, W. Zhou, W. Zhao, S. Fan, K. Jiang, Epitaxial growth of aligned and continuous carbon nanofibers from carbon nanotubes, ACS Nano 11 (2017) 1257–1263.
[11] G.B. Zheng, H. Sano, Y. Uchiyama, A layer-by-layer deposition mechanism for producing a pyrolytic carbon coating on carbon nanotubes, Carbon 57 (2013) 267–273.
[12] K. Li, G. Eres, J. Howe, Y.J. Chuang, X. Li, Z. Gu, L. Zhang, S. Xie, Z. Pan, Self--assembly of graphene on carbon nanotube surfaces, Sci. Rep. 3 (2013) 2353.
[13] Y. Jin, Y. Zhang, Q. Zhang, R. Zhang, P. Li, F. Wei, Multi-walled carbon nanotube-based carbon/carbon composites with three-dimensional network structures, Nanoscale 5 (2013) 6181–6186.
[14] J. Lee, T. Kim, Y. Jung, K. Jung, J. Park, D.M. Lee, H.S. Jeong, J.Y. Hwang, C.R. Park, K.H. Lee, S.M. Kim, High-strength carbon nanotube/carbon composite fibers via chemical vapor infiltration, Nanoscale 8 (2016) 18972–18979.
[15] N. He, O. Yildiz, Q. Pan, J. Zhu, X. Zhang, P.D. Bradford, W. Gao, Pyrolytic-carbon coating in carbon nanotube foams for better performance in supercapacitors, J. Power Sources 343 (2017) 492–501.
[16] R. Jacobsen, M. Monthioux, Carbon beads with protruding cones, Nature 385 (1997) 211–212.
[17] H. Allouche, M. Monthioux, R.L. Jacobsen, Chemical vapour deposition of pyrolytic carbon on carbon nanotubes. Part 1: synthesis and morphology, Carbon 41 (2003) 2897–2912.
[18] H. Allouche, M. Monthioux, Chemical vapour deposition of pyrolytic carbon on carbon nanotubes. Part 2: texture and Structure, Carbon 43 (2005) 1265–1278.
[19] M. Monthioux, H. Allouche, R.L. Jacobsen, Chemical vapour deposition of pyrolytic carbon on carbon nanotubes. Part 3: growth mechanism, Carbon 44 (2006) 3183–3194.
[20] G. Paredes, G. Seine, R. Cours, F. Houdellier, H. Allouche, T. Ondarçuhu, F. Piazza, M. Monthioux, Synthesis and (some) applications of carbon-nanotube–supported pyrolytic carbon nanocones, Indian J. Eng. Mater. Sci. 27 (2020) 1091–1094.
[21] K. Reichelt, Nucleation and growth of thin films, Vacuum 38 (1988) 1083–1099.
[22] C. Ratsch, J.A. Venables, Nucleation theory and the early stages of thin film growth, J. Vac. Sci. Technol. A 21 (2003) S96–S109.
[23] J.A. Venables, G.D.T. Spiller, Nucleation and growth of thin films, in: V.T. Binh (Ed.), Surface Mobilities on Solid Materials: Fundamental Concepts and Applications, Springer-Verlag, 1983, pp. 341–403.
[24] E. Bouchard, J. Lavenac, J.C. Roux, F. Langlais, P. Delhaès, Pyrocarbon deposits on a graphite surface observed by STM, Chem. Vap. Depos. 7 (2001) 125–130.
[25] F. Soutric, M. Monthioux, E. Musset, J.F. Després, Low temperature pyrolytic carbon films: preparation and TEM investigations, Proc. Eurocarbon Conf. 2 (1998) 653–654 Strasbourg, France.
[26] W.J. Lee, C. Li, J. Gunning, N. Burke, J. Patel, Is the structure of anisotropic pyrolytic carbon a consequence of growth by the Volmer-Weber island growth mechanism? Carbon 50 (2012) 4773–4780.
[27] Z.T. Hu, K.J. Huttinger, Mechanism of carbon deposition – a kinetic approach, Carbon 40 (2002) 624–628.
[28] G.L. Dong, K.J. Hüttinger, Consideration of reaction mechanisms leading to pyrolytic carbon of different textures, Carbon 40 (2002) 2515–2528.
[29] Z.J. Hu, B. Reznik, W.G. Zhang, D. Gerthsen, K.J. Huttinger, Influence of pressure, temperature and surface area/volume ratio on the texture of pyrolytic carbon deposited from methane, Carbon 41 (2003) 749–758.
[30] M.W. Chen, Y.B. Zhu, J. Xia, H.A. Wu, Molecular insights into the initial formation of pyrolytic carbon upon carbon fiber surface, Carbon 148 (2019) 307–316.
[31] R.O. Grisdale, The formation of black carbon, J. Appl. Phys. 24 (1953) 1082–1091.
[32] K. Koizlik, J. Linke, H. Luhleich, H. Nickel, P. Pflaum, Contribution to the pyroaggregate hypothesis and the droplet model of pyrocarbon deposition, in: k.Koizlik (Ed.), Contribution to the development of reactor graphites and pyrocarbons-Irradiation behavior, model conceptions and characterization, in: Proceedings of the 4th London International Carbon and Graphite Conference, 1974, pp. 34–46. Sept 23-27, Jülich.
[33] L.H. Ford, C.F. Bilsby, Porosity related to structure for low temperature propylene pyrocarbones, J. Nucl. Mater. 60 (1976) 79–88.
[34] J.H. Je, J.Y. Lee, A study of the deposition of pyrolytic carbons from hydrocarbons, Carbon 22 (1984) 563–570.
[35] R. Shi, H.J. Li, Z. Yang, M.K. Kang, Deposition mechanism of pyrolytic carbons at temperature between 800 and 1200 °C, Carbon 35 (1997) 1789–1792.
[36] K. Lafdi, S. Bonnamy, A. Oberlin, Mechanism of anisotropy occurrence in a pitch precursor of carbon fibers: part I-Pitches A and B, Carbon 29 (1991) 831–847.
[37] E. Dujardin, T.W. Ebbessen, H. Hiura, K. Tanigaki, Capillarity and wetting of carbon nanotubes, Science 265 (1994) 1850–1852.
[38] M.H. Wagner, H. Jäger, I. Letizia, G. Wilhelmi, Quality assessment of binder pitches for carbon and graphite electrodes, Fuel 67 (1988) 792–797.
[39] I. Mochida, Y. Korai, C.H. Ku, W. Watanabe, Y. Sakai, Chemistry of synthesis, structure, preparation and application of aromatic-derived mesophase pitch, Carbon 38 (2000) 305–328.
[40] V.G. Rocha, C. Blanco, R. Santamaria, E.I. Diestre, R. Menendez, M. Granda, Pitch/coke wetting behavior, Fuel 84 (2005) 1550–1556.
[41] O.N. Shornikova, A.P. Malakho, A.M. Kenigfest, V.V. Kulakov, A.N. Seleznev, V.V. Avdeev, Wetting of carbon fibers by coal-tar pitch melts, Fiber Chem. 44 (2012) 259–264.
[42] O. Atteia, Modélisation Du Devenir Des Composés Organiques Dans Les Aquifères, Lavoisier, Paris, France, 2011.
[43] B.J. Carroll, Equilibrium conformations of liquid drops on thin cylinders under forces of capillarity. A theory for the roll-up process, Langmuir 2 (1986) 248–250.
[44] H.B. Eral, J. de Ruiter, R. de Ruiter, J.M. Oh, C. Semprebon, M. Brinkmann, F. Mugele, Drops on functional fibers: from barrels to clamshells and back, Soft. Matter. 7 (2011) 5138–5143.
[45] J.M. Ting, J.B.C. Lan, Beaded carbon tubes, Appl. Phys. Lett. 75 (1999) 3309–3311.
[46] J.M. Ting, B.C. Lan, Formation of nodulated vapor grown carbon fiber, Carbon 38 (2000) 1917–1923.
[47] J. Eggers, E. Villermaux, Physics of liquid jets, Rep. Prog. Phys. 71 (2008) 036601.
[48] P.G. de Gennes, F. Brochart-Wyart, D. Quéré, G., Bulles, Perles, et Ondes, Belin, Paris, France, Collection Echelles, 2005.
[49] S. Mora, T. Phou, J.-.M. Fromental, L.M. Pismen, Y. Pomeau, Capillarity driven instability of a soft solid, Phys. Rev. Lett. 105 (2010) 21401.
[50] B.J. Carroll, The accurate measurement of contact angle, phase contact areas, drop volume, and Laplace excess pressure in drop-on-fiber systems, J. Colloid. Interface Sci. 57 (1976) 488–495.
[51] D. Quéré, Fluid coating on a fiber, Ann. Rev. Fluid Mech. 31 (1999) 247–384.
[52] S.L. Goren, The shape of a thread of liquid undergoing break-up, J. Coll. Sci. 19 (1964) 81–86.
[53] S. Haefner, M. Benzaquen, O. Bäumchen, T. Salez, R. Peters, J.D. McGraw, K. Jacobs, E. Raphaël, K.D. Veress, Influence of slip on the Plateau–Rayleigh instability on a fiber, Nat. Commun. 6 (2015) 7409.
[54] J. Dolado, K.L. Renforth, J.E. Nunn, S.A. Hindsmarsh, P. Hidalgo, A.M. Sanchez, B. Méndez, Zn_2GeO_4/SnO_2 nanowire heterostructures driven by Plateau-Rayleigh instability, Cryst. Growth Des. 20 (2020) 506–513.
[55] F.M. Kolb, H. Hofmeister, M. Zacharias, U. Gösele, On the morphological instability of silicon/silicon dioxide nanowires, Appl. Phys. A 80 (2005) 1405–1408.
[56] S.U. Setru, B. Gouveia, R. Alafaro-Aco, J.W. Shaevitz, H.A. Stone, S.A. Petry, Hydrodynamic instability drives protein droplet formation on microtubules to nucleate branches, Nat. Phys. 17 (2021) 493–498.
[57] A. Dekeyrel, Mise Au Point D'un Procédé D'élaboration Rapide De Composites

Carbone/Carbone Haute Densité, PhD Dissertation, University of Bordeaux 1, 2010 France.
[58] H. Fong, I. Chun, D.H. Reneker, Beaded nanofibers formed during electrospinning, Polymer 40 (1999) 4585–4592.
[59] M. Moseler, U. Landman, Formation, stability, and breakup of nanojets, Science 289 (2000) 1165–1169.
[60] C. Zhao, J.E. Sprittles, D.A. Lockerby, Revisiting the Rayleigh-Plateau instability for the nanoscale, J. Fluid Mech. 861 (2019) R3.1–R3.11.
[61] S. Chen, Y. Feng, M. Qin, T. Ji, W. Feng, Improving thermal conductivity in the through-thickness direction of carbon fiber/SiC composites by growing vertically aligned carbon nanotubes, Carbon 116 (2017) 84–93.
[62] C. Bourgerette, A. Oberlin, M. Inagaki, Structural and textural changes from polyimide Kapton to graphite: part I, J. Mater. Res. 7 (1992) 1158–1173.
[63] W.A. de Heer, P. Poncharal, C. Berger, J. Gezo, Z. Song, J. Bettini, D. Ugarte, Liquid carbon, carbon-glass beads, and the crystallization of carbon nanotubes, Science 307 (2005) 907–910.
[64] E. Lorenceau, D. Quéré, Drops on a conical wire, J. Fluid Mech. 510 (2004) 29–45.
[65] Y. Zheng, H. Bai, Z. Huang, X. Tian, F.Q. Nie, Y. Zhao, J. Zhai, L. Jiang, Directional water collection on wetted spider silk, Nature 463 (2010) 640–643.
[66] R. Shi, Y. Tian, L. Wang, Bioinspired fibers with controlled wettability: from spinning to application, ACS Nano 15 (2021) 7907–7930.